Environ. Sci. Technol. **2001**, *35,* 3169−3174

Chromium Diffusion and Reduction in Soil Aggregates

TETSU K. TOKUNAGA,*,† JIAMIN WAN,† MARY K. FIRESTONE,‡ TERRY C. HAZEN,† EGBERT SCHWARTZ,‡ STEPHEN R. SUTTON,§ AND MATTHEW NEWVILLE§

Lawrence Berkeley National Laboratory, Berkeley, California 94720, University of California, Berkeley, California 94720, and University of Chicago, Chicago, Illinois 60637

The distribution of metal contaminants such as chromium in soils can be strongly localized by transport limitations and redox gradients within soil aggregates. Measurements of Cr(VI) diffusion and reduction to Cr(III) were obtained in soil columns representing transects into soil aggregates in order to quantify influences of organic carbon (OC) and redox potentials on Cr transport distances and microbial community composition. Shifts in characteristic redox potentials, and the extent of Cr(VI) reduction to Cr(III) were related to OC availability. Depth profiles of Cr(VI, III) obtained with micro X-ray absorption near edge structure (micro-XANES) spectroscopy reflected interdependent effects of diffusion and spatially dependent redox potentials on reduction kinetics and microbial community composition. Shallow diffusion depths (2−10 mm) and very sharply terminated diffusion fronts in columns amended with OC (80 and 800 ppm) reflected rapid increases in Cr reduction kinetics over very short (mm) distances. These results suggest that Cr contamination in soils can be restricted to the outsides of soil aggregates due to localized transport and rapid reduction and that bulk sample characterization is inadequate for understanding the controlling biogeochemical processes.

Introduction

Chromium is one of the most common metal contaminants in soils because of its use in metal plating, tanneries, wood preservation, and pigmentation (*1, 2*). In soil and groundwater systems, Cr exists in the III and VI oxidation states, with the majority of Cr(III) species being stable solids or more strongly adsorbed species, and the majority of Cr(VI) species being more soluble and mobile (*3*). Transport and reactions of chromium in soils and groundwaters are of concern because of the toxic and carcinogenic effects of Cr(VI). Because of the high pe range associated with Cr(VI)−Cr(III) transition, most Cr in uncontaminated soils is found as Cr(III), and high proportions of Cr(VI) are largely restricted to contaminated sites. Cr(VI) transport and reduction in such contaminated soils ultimately reflect interdependent influences of physical, geochemical, and microbial processes. Prior to reduction, Cr(VI) entering a soil may remain in solution, adsorb onto solid surfaces, or precipitate. Like other oxyanions, retardation of Cr(VI) transport by adsorption is strongly pH dependent and weak under alkaline conditions (*4*).

A number of abiotic reactions may be responsible for the transformation of Cr(VI) to Cr(III) in soils. In soil solutions, Fe(II), S(−II), and various organic compounds including fulvic and humic acids have been shown to reduce Cr(VI) (*5*−*9*). Reduction of Cr(VI) on surfaces of Fe(II) solids (biotite, Fe(II) impurities in α-FeOOH, FeS, magnetite, ilmenite, green rusts) has been investigated (*10*−*16*). Common soil minerals such as TiO_2, Al_2O_3, FeOOH, montmorillonite, and kaolinite have been shown to catalyze Cr(VI) redox reactions with organic compounds and Fe(II) (*17*−*19*). Microorganisms can reduce Cr(VI) in soil by both direct and indirect mechanisms. Indirect microbial Cr reduction proceeds through depletion of oxygen, reduction of Fe and S (*20, 21*), and production of organic ligands and reductants. Direct microbial enzymatic reduction of Cr(VI) in soils has also been reported (*22*−*24*). A comparison of abiotic versus enzymatic Cr(VI) reduction kinetics indicates that the abiotic pathways are expected to be dominant in most soils under reducing conditions (*25*). Nonetheless, soil biological influences are expected to remain dominant, through promoting the indirectly microbial Cr reduction processes mentioned above.

The response of a field soil profile to a Cr(VI) contamination event is complicated because of interrelated physical, chemical, and biological processes, occurring over a wide range of length and time scales. For purposes of identifying and quantifying specific mechanisms and processes, most studies to date on the soil biogeochemistry of Cr have been conducted in homogeneous batch systems. Yet soils typically are heterogeneous, composed of aggregates, and contain preferential flow paths, such that the early stages of a contamination event are usually in disequilibria with respect to transport and reactions. In such structured soils, it is expected that contaminants rapidly move through a small subset of hydraulically active macropores and slowly diffuse into the adjacent soil aggregates. Such a scenario is the basis for applying two-region (mobile and immobile) models to describe solute transport, in which advection is limited to the mobile domain, and the immobile domain participates through diffusive mass transfer (*26, 27*). Some studies have successfully modeled Cr breakthrough in effluents collected from soil columns using various versions of the two-region approach (*28, 29*). Although it has recently been shown that the dichotomy between advective and diffusive regions is often not well-defined, with fitting parameters being dependent on flow rate and saturation (*30*), the two-region approach remains a useful starting point for description of transport in structured media. However, it should be noted that the vast majority of studies that have applied two-region models to describe transport through soil columns have done so without any direct measurements within the immobile, aggregate domain.

To better understand reactive transport of redox-sensitive species such as Cr in structured soils, it is essential to obtain information on transport-limited, intra-aggregate biogeochemical dynamics. Outer surfaces of soil aggregates tend to sustain oxidizing conditions favoring stability of Cr(VI), whereas interior regions are more reducing, promoting conversion to Cr(III). The level of microbial activity within aggregates is critical in controlling the extent of Cr(VI) reduction, whether directly through enzymatic pathways or through indirect influences involving control of intra-aggregate redox potentials and resulting concentrations of

* Corresponding author phone: (510)486-7176; fax: (510)486-7797; e-mail: tktokunaga@lbl.gov.
† Lawrence Berkeley National Laboratory.
‡ University of California.
§ University of Chicago.

10.1021/es010523m CCC: $20.00
Published on Web 07/03/2001

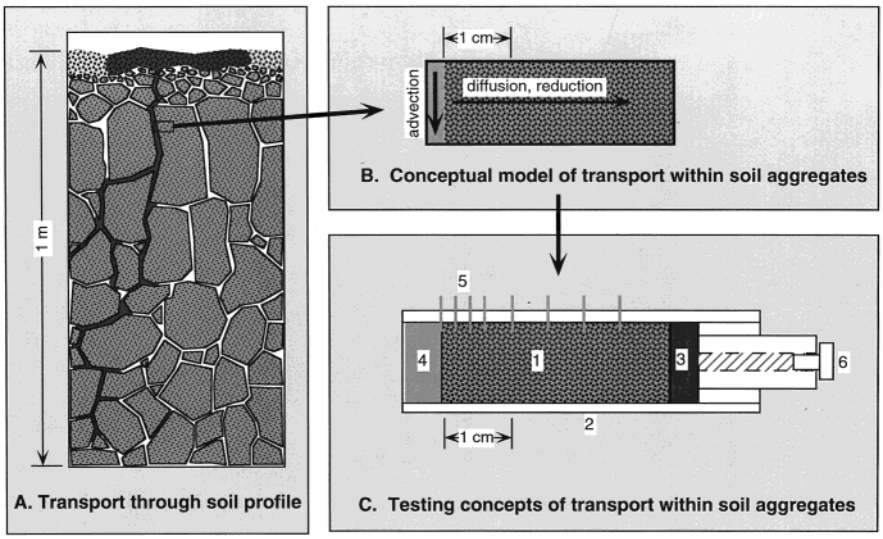

FIGURE 1. Conceptual models of reactive transport in field soil profiles and in soil aggregates, and model testing. (a) Preferential flow and transport from the soil surface toward groundwater, strongly influenced by macropore (fracture) pathways. (b) Two-region model, with advection-dominated transport through macropores, and diffusion-limited reactions within soil aggregates. (c) Experimental system for measuring metal contaminant diffusion and reduction within synthetic soil aggregates. Components of these laboratory aggregate microcosms include (1) synthetic soil aggregate, (2) acrylic cylinder, (3) syringe piston with central port, (4) "macropore" reservoir, (5) platinum wire redox electrodes, and (6) plug. One side section of the acrylic cylinder (5 mm wide by 35 mm long) is cut away and resealed with Kapton film to permit micro-XANES mapping.

abiotic reductants [Fe(II), S(−II), and organic carbon]. In general, the intra-aggregate domain may not be even approximately homogeneous with respect to microbial communities, redox potentials, and reactivity to contaminants. For these reasons, reactive transport studies on single soil aggregates can help identify where specific processes (understood through studies of well-mixed batch systems) occur within more complex systems. This work focuses on the problem of Cr(VI) transport within columns designed to represent transects into soil aggregates (Figure 1) in order to determine length and time scales over which reduction to Cr(III) occurs under diffusion-limited conditions.

Materials and Methods

The soil, Altamont clay (Aridic Haploxerert), was collected from Altamont Pass (Alameda County, CA) on two different sampling trips, with sampling locations separated by a lateral distance of 0.7 m. Preliminary experiments were conducted on the first soil sample, denoted S1. The main portion of this study was conducted on the second sample, denoted S2. Samples of blocky C horizon (0.2−0.5 m depth) aggregates were crushed, homogenized, and packed into microcosms. Soils were calcareous (0.8−4.2% $CaCO_3$, pH 8.5) and clayey in texture (40−55% mass particles $\leq$ 2 μm, primarily as smectite and kaolinite). The S1 and S2 soils contained different amounts of native Cr, 150 ($\pm$10) and 64 ($\pm$5) ppm, respectively. This native Cr was largely ($\geq$95%) in Cr(III) forms, as determined by XANES (X-ray absorption near edge structure) analyses described below, with less than 0.2% of the total Cr in either water- or phosphate-extractable forms. The soil aggregate microcosms were of two types. One set of microcosms was contained in chambers similar to those used in a previous Se reactive transport study (*31*). These synthetic aggregates were typically 30 mm in length, 10 mm in width, and about 5 mm in thickness. The other type of microcosms were contained in modified 5 mL syringes and packed to a length of 30 mm. Both types of microcosms were equipped with Pt electrode arrays (2−5 mm spacing) for redox potential measurements and Kapton windows for micro-XANES measurements described below. Bulk densities and porosities of these synthetic aggregates were 1.34 Mg m^{-3} and 0.50, respectively. The long (30 mm) dimension represents a transect into a soil aggregate, with an aerobic boundary at one end, and a potentially anaerobic core region on the opposite end (Figure 1). The soils were saturated with a neutral salt (5 mM KCl, 5 mM $CaSO_4$), or a 80 ppm organic carbon (OC) solution, or a 800 ppm OC solution. Tryptic soy broth (TSB) was used as the OC supplement since it is a plant product, and its composition may mimic a carbon source that the indigenous microbial community is exposed to. These soils had about 1% native OC, and the OC-amendment added to soils was intended to stimulate more rapid microbial growth, hence more reducing conditions. Redox potential measurements were begun within several hours after aggregates were wetted, using the embedded Pt electrodes and a calomel reference microelectrode (*31, 32*).

Following 14 days of incubation at room temperature (19−22 °C), the exterior boundary of each microcosm was exposed to a Cr(VI) solution for either 3 or 11 days, simulating an episodic contamination event (only the +0 ppm OC and +800 ppm OC S1 soils in contact with 1,000 ppm Cr(VI) received 11 days of exposure). The majority of the microcosms (all S2 and some S1 series) were exposed to an initial Cr(VI) concentration of 1000 ppm. Additional microcosms (S1) were exposed to 260 and 5200 ppm Cr(VI). The Cr(VI) exposure event consisted of a single application (ponding) of a finite volume of K_2CrO_4 solution at the aerobic boundary ($x = 0$ in Figure 1). The outlet plug was kept sealed during and after the Cr application in order to ensure that transport was diffusive. At the end of this exposure period, the ponded solution was removed and analyzed using the diphenylcarbazide (DPC) method (*33*) to determine the amount of Cr transported into the soil.

Microbial communities were characterized before and after Cr exposure, so that possible community responses to this contaminant could be identified. Three sets of additional syringe-type aggregate microcosms, without Pt electrodes and Kapton windows, were prepared for extrusion of column sections for these microbiological studies. Each of these three sets was sampled at a different time, immediately prior to Cr exposure (at 14 days of incubation), immediately after 3 days of Cr exposure, and 13 days after Cr exposure. The

extruded cores were cut into 3 mm lengths for the two segments closest to the exposure boundary and into 6 mm segments over the remainder of each core. DNA was extracted with the BIO 101 soil DNA extraction kit (BIO 101) from each segment in microcosms exposed to 1000 ppm Cr(VI) and previously wet with either 800 ppm OC solution or a dilute salt solution. Intergenic Transcribed Spacer (ITS) patterns were constructed by performing PCR reactions with the following ingredients: approximately 10 ng of soil DNA, 10 pmol each of the primers 115R and 1406F, 12.5 nmol of dNTP, 1X PCR buffer, 750 nmol of $MgCl_2$, and 2.5 units of Taq polymerase in a total volume of 25 μL. The PCR program started with a 3 min hot start at 92 °C, followed by 30 cycles of 30 s of melting at 92 °C, 30 s annealing at 55 °C, and 1 min of extension at 72 °C. The reaction was completed with a final extension step for 7 min at 72 °C. Five microliters of this reaction was analyzed on a 16 cm long 5%, 1X TAE polyacrylamide gel, which was run for 5 h at 150 v. The gel was stained with SYBR green I and photographed with a Kodak DC120 digital camera. A cluster analysis of the gel patterns was constructed by analyzing the digital image with the program Gelcompare. Direct microscopic analysis of sediments for total number of cells per gram of soil wet weight were measured using Live/Dead BacLight Bacterial Viability Kit (L-7007). One gram of soil is suspended in 9 mL of pyrophosphate buffer (1 g $Na_4P_2O_7$ H_2O/L dH_2O). After vortexing for 1 min, the mixture is allowed to stand for 5 min. Ten milliliters is spread onto the well of a toxoplasmosis microscope. The slides are dried at room temperature and stained according to the kit instructions. Counts are done with a Zeiss epifluorescent microscope by counting the total number of fluorescing cells.

Most of the Cr measurements were obtained using XANES spectroscopy, with supplemental information from bulk X-ray fluorescence and DPC analyses. Micro-XANES measurements were obtained at the Advanced Photon Source (Argonne National Laboratory, Argonne, IL), on the GeoSoilEnviroCARS beamline 13ID-C. For the purpose of Cr oxidation state determination, the monochromator was cycled through energies of −10, 0, and +40 eV relative to the distinct Cr(VI) preedge peak energy (5993 eV). This procedure alone permits determinations of amounts of Cr(VI) relative to total Cr [denoted Cr(VI)/$\sum$Cr] through measured intensities of the preedge (0 eV) absorption normalized to the above edge (+40 eV) absorption. Small background absorption at −10 eV was subtracted from both preedge and above-edge absorption prior to normalization. Details of this and similar procedures have been described in many previous studies on Cr XANES (*10, 14, 15, 34*−*37*). Cr(VI) standard samples were periodically run through the same cycle of three energies in order to check the monochromator energy calibration. The absolute monochromator calibration is good to about 0.1 eV, which corresponds to a potential uncertainty in Cr(VI)/$\sum$Cr of 4%. The X-ray absorption at 40 eV above the preedge peak energy by itself does not permit quantification of the total Cr concentration because of significantly different oscillations in the Cr(VI) and Cr(III) absorption spectra in this region. Therefore, the dependence of absorption at 40 eV on the Cr(VI)/$\sum$Cr ratio was determined from X-ray absorption spectra of Cr(VI) and Cr(III) standards normalized to absorption at relative energies in excess of 90 eV, where differences in absorption due to oxidation state are small. Total Cr concentration calibrations were obtained from X-ray fluorescence measurements of the unspiked Altamont S2 and S1 soils (64 and 150 ppm Cr, respectively) and a NIST standard of similar elemental composition (San Joaquin soil, 130 ppm Cr).

Micro-XANES transects across the synthetic aggregates were obtained by moving the sample in front of the stationary beam in 0.25−0.5 mm steps using a motorized stage. Although a much finer spatial resolution (1 μm) is possible on this beamline, a defocused X-ray beam of 250 μm (vertical) by 700 μm (horizontal) was used for this study. Samples were mounted such that the long axis of the beam was perpendicular to the aggregate depth axis. The larger spot size was selected (i) in order to volume-average over a sufficient number of soil particles and pores, (ii) because of the moderately large CrO_4^{2-} diffusivity in these sediments, and (iii) to minimize X-ray induced Cr(VI) reduction. This latter artifact was kept to less than 5%, based upon separate time-dependent tests. The Cr(VI) to total Cr ratio at a given location was determined from its approximately linear relation to the normalized preedge peak height. Small variations in measured X-ray fluorescence arose from slight variations in the orientation of the Kapton window-covered soil surfaces since they were not perfectly flat. To compensate for these orientational variations, Ti K-α X-ray fluorescence profiles were also collected and used to normalize the total Cr profiles. Titanium, as TiO_2, is practically inert and uniformly distributed in these synthetic soil aggregates (at the $\approx$300 μm measurement scale). This normalization was effective because the X-ray beam is very large relative to the characteristic grain-size (<2 μm).

To test the extent of abiotic Cr reduction, we measured water-extractable Cr(VI) in γ-irradiated and autoclaved soils that were either amended with 800 ppm OC or a dilute salt solution and then spiked with Cr(VI). No Cr(VI) reduction was observed in either treatment, indicating TSB without the aid of microorganisms could not promote Cr(VI) reduction. Other batch experiments on Cr(VI) mixed with TSB into Altamont soil without previously establishing reducing conditions showed negligible Cr reduction, indicating that neither the OC supplement nor indigenous microbial population were capable of reducing Cr at rates that were competitive with those observed in the aggregates.

Other short-term (1−24 h) batch tests of the Altamont clay soil were run to determine whether sorption of added Cr(VI) would be important. Batch sorption tests at low Cr(VI) concentrations (0−10 ppm) on the Altamont clay yielded very low linear sorption coefficients in the range of 0.04−0.1, indicating that retardation of the CrO_4^{2-} diffusion front by adsorption onto minerals was minor. Sorption of oxyanions in alkaline soils is commonly very weak because of lack of protonated mineral surface sites.

Results and Discussion

Redox potential profiles stabilized within 10−14 days relative to initial wetting. The redox potential profiles measured after exposure to Cr(VI) are shown in Figure 2. Generally, profiles in systems with higher OC addition exhibited overall lower redox potentials and lower potentials at greater depths. Slightly elevated redox potentials at the deep end of the S2, 80 ppm OC system (Figure 2B) might have been caused by entrapped air in the outflow port. Approximate ranges of measured potentials associated with key redox transitions [Cr(VI)−Cr(III), Mn(IV)−Mn(II), Fe(III)−Fe(II), and S(VI)−S(−II)] are shown in Figure 2D for comparison with these profiles (*38, 39*). The steep redox potential gradients measured in the +80 ppm OC aggregates (Figure 2D) would support steeply increasing concentrations of Fe(II) and S(−II) with depth. Kinetic studies of Cr(VI) reduction by $Fe(II)_{aq}$ indicate that this is likely to be the dominant pathway under the alkaline-reducing conditions of these soils (*25, 40, 41*). Following addition of CrO_4^{2-}, increases in redox potentials propagated inward from the exposure surface. Factors responsible for differences between the stable S1 (Figure 2D) and S2 (Figure 2B) redox profiles prior to Cr exposure (day 0.0) have not been identified. Although both soils were infused with 80 ppm OC solutions, the S1 microcosm was significantly more reducing. Differences in the redox potential profile

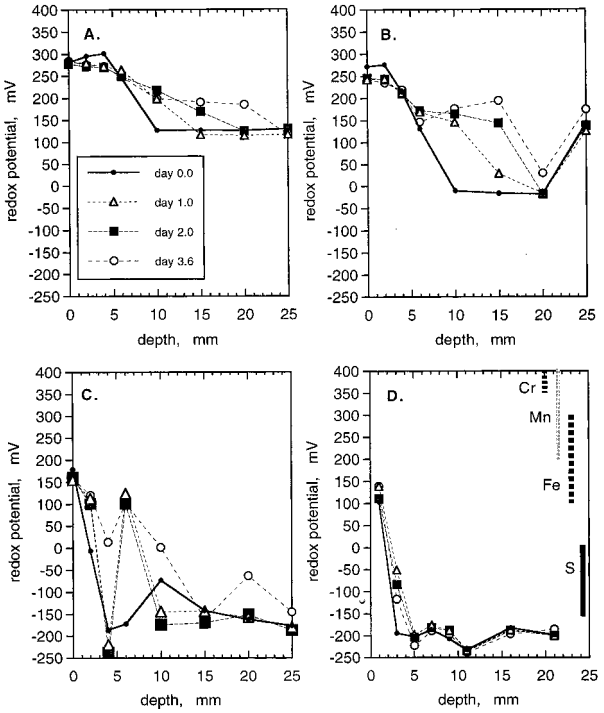

FIGURE 2. Redox potential (referenced to the standard H electrode) profiles within aggregates, at various times since exposure to Cr-(VI). The profiles are from (a) S2 soil without additional organic carbon (OC), (b) S2 soil presaturated with +80 ppm OC solution, (c) S2 soil presaturated with +800 ppm OC solution, and (d) S1 soil presaturated with +80 ppm OC solution. The S2 soils were all exposed to 1000 ppm Cr(VI) at the boundary (depth = 0 mm). The S1 soil was exposed to 260 ppm Cr(VI). Nominal experimental redox potential ranges associated with Cr(VI, III), Mn(IV, II), Fe(III, II), and S(VI, −II) transitions are indicated in panel d.

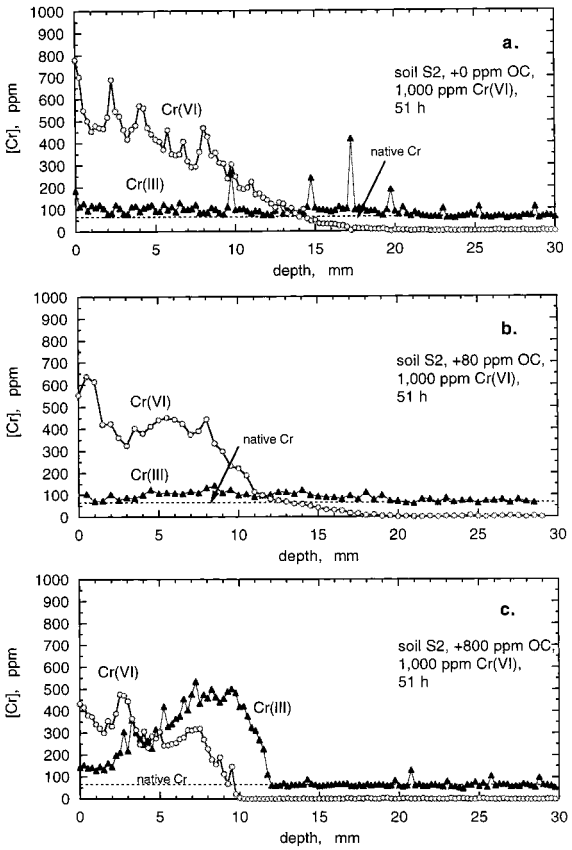

FIGURE 3. Micro-XANES profiles of Cr(VI) and Cr(III) in the S2 soil at 51 (±1) hours since exposure to 1000 ppm Cr(VI). The profiles are from aggregates presaturated with (a) +0 ppm OC, (b) +80 ppm OC, and (c) +800 ppm OC. The background native Cr of the S2 soil is 64 ppm (>95% as Cr(III)). The relative uncertainty in concentrations is about 9%.

responses to Cr exposure in these two systems, both supplied with +80 ppm OC solutions, probably reflect slight differences in original soil sample batches as well as differences in entrapped air (oxygen) during initial wetting and in boundary Cr(VI) concentrations.

Micro-XANES transects taken at 51 h (Figure 3) of the three (0, +80 ppm, and +800 ppm OC) S2 microcosms exposed to 1000 ppm Cr(VI) show +0 and +80 ppm OC systems responded fairly similarly with respect to Cr transport and reduction. Much shorter Cr penetration distances were observed in aggregates amended with the highest amounts of OC (+800 ppm). Although a smaller region of the high OC aggregate was contaminated, it received a higher influx of Cr. Larger amounts of Cr diffuse into more highly reducing aggregates because its rapid reduction within short distances sustains higher Cr(VI) concentration gradients, hence higher diffusive fluxes. The highly reducing (high OC) aggregate also exhibited abrupt termination of the diffusion front, reflecting diffusion into a system in which the Cr reduction rate increases rapidly with depth. In these graphs and ones to follow, all soil Cr concentrations are referenced to the local soil dry mass. Comparisons between Cr influxes measured from X-ray fluorescence microprobe profiles of soils and DPC measurements on Cr losses from pool solutions were within 10% agreement for all systems except for the S2, +80 ppm OC microcosm. The discrepancy in this case amounted to X-ray measured Cr influxes being 34% higher than DPC measured Cr losses from the reservoir.

Profiles from later times (11 and 23 days) indicate higher Cr(VI) concentrations were maintained along exterior portions of aggregates (Figure 4). This is significant because this unreduced fraction resides along potential flow pathways and hence remains more susceptible to advective transport. It is anticipated that at still later times, Cr(VI) will diffuse further into aggregates and eventually become reduced. However, some Cr(VI) may persist in highly stable, low solubility solids such as $BaCrO_4$, $Ba(S, Cr)O_4$, and $PbCrO_4$ (*3, 37, 42*). The extent of Cr(VI) precipitation with Ba is likely to be more important than precipitation with Pb in the Altamont soils (745 ± 20 ppm, and 50 ± 20 ppm, respectively, measured by bulk X-ray fluorescence analysis).

Factor(s) responsible for the development of locally very high concentrations within the general Cr(III) precipitation zones have not been identified. However, the most prominent location of Cr accumulation centered at a depth of 6.0 mm in the S1 soil exposed to 5200 ppm Cr(VI) coincided with the most obvious of dark mottled spots developed during sample incubation and visible through the Kapton window (Figure 5). Supplemental X-ray fluorescence measurements indicated that the Mn concentration in this location is about 6 times higher than that of the bulk soil. Rhodochrosite ($MnCO_3$) is the stable Mn(II) mineral associated with the alkaline-reducing conditions of this soil, but micro X-ray diffraction measurements were not obtained.

Although redox potential measurements in soils and natural waters commonly only provide qualitative information, some studies have concluded that they can be quite informative in environments where the Fe(III)/Fe(II) couple exerts a dominant influence (*43, 44*). This possibility was examined in our systems, based on the assumption that Fe-(II) was the dominant reductant for Cr(VI). The depth of penetration of the oxidation front at specific times, as measured by increases in Pt electrode potentials, was

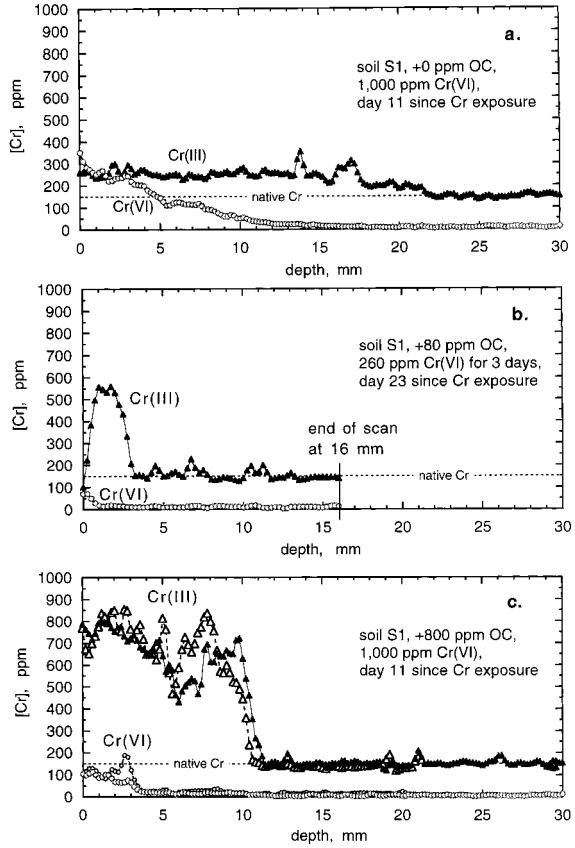

FIGURE 4. Micro-XANES profiles of Cr(VI) and Cr(III) in the S1 soil at later times (11 and 23 days) since exposure to Cr(VI). The profiles are from aggregates presaturated with (a) +0 ppm OC, (b) +80 ppm OC, and (c) +800 ppm OC (2 profiles shown). The +0 and +800 ppm OC aggregates were exposed to 1000 ppm Cr(VI). The +80 ppm OC aggregates was exposed to 260 ppm Cr(VI). The background native Cr of the S1 soil is 150 ppm (>95% as Cr(III)). The relative uncertainty in concentrations is about 9%.

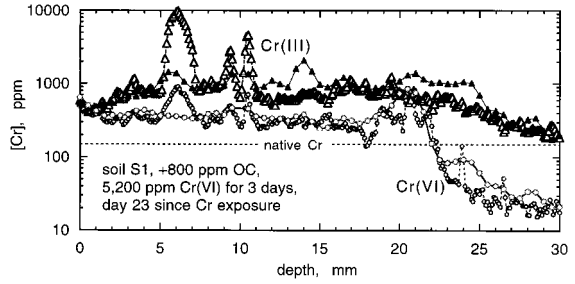

FIGURE 5. Two micro-XANES profiles of Cr(VI) and Cr(III) in the +800 ppm OC, S1 soil at 23 days since exposure to 5,200 ppm Cr(VI).

compared with micro-XANES measured depths of the Cr diffusion front (Figure 6). The fair agreement between these two measurements is supportive of the importance of Fe-$(II)_{aq}$ in reducing Cr(VI) in these soils.

Microbial population densities, as measured with direct count microscopic methods, were generally high. More microorganisms were present in soils amended with 800 ppm OC (2×10^8 cells g^{-1} soil) than in unamended soil (7×10^7 cells g^{-1} soil). DNA fingerprints showed the bacterial community composition varied along the column. Gel patterns of columns, not amended with OC, and columns to which 800 ppm OC was added showed communities in samples exposed to Cr(VI) clustered separately from samples that were not exposed (Figure 7). This pattern corresponds well with the micro-XANES analysis and suggests Cr(VI) exposure

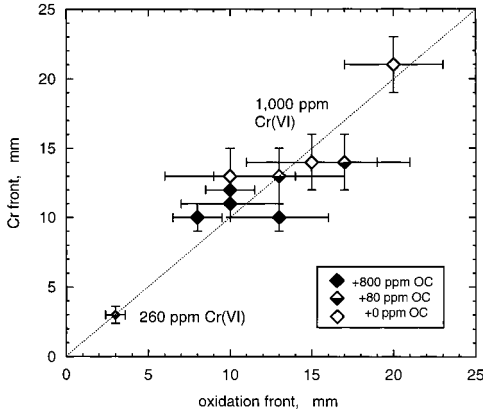

FIGURE 6. Correlation between the location of the oxidation front and Cr diffusion front within aggregates. Bars indicate uncertainty ranges. The root mean-square deviation of data points from the 1:1 line is 1.9 mm.

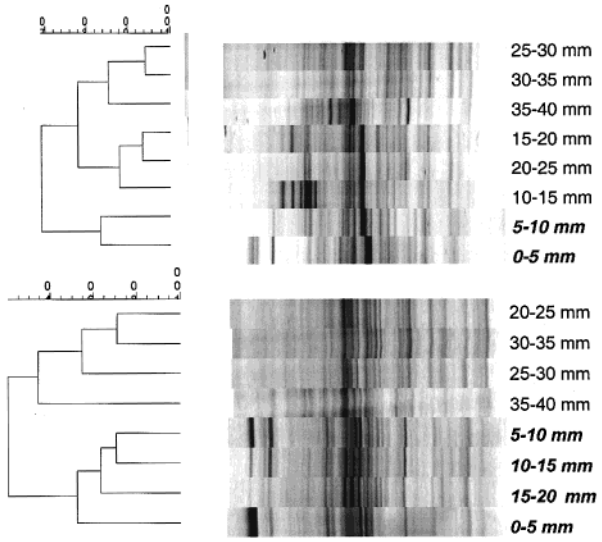

FIGURE 7. Cluster analysis of ITS patterns from columns either amended with 800 ppm OC (top) or a dilute salt solution (bottom). Labels to the right of the gel patterns refer to the distance from the original Cr(VI) source that the samples were taken. Samples exposed to Cr (VI) according to micro-XANES analysis are in bold italics.

had a strong impact on the composition of the bacterial community.

In general, the depth of Cr transport into aggregates was less than expected by diffusion without reduction, inversely related to OC amendment, and proportional to the boundary Cr(VI) concentration. These results show how a metal contaminant, Cr(VI), can become very locally reduced within soil aggregates, depending on redox conditions established by microorganisms. Microbial respiration combined with low O_2 diffusivities in nearly water-saturated soils results in elevated $Fe(II)_{aq}$ and low redox potentials in interior regions of aggregates. In systems with high available OC and high microbial activity, Cr reducing conditions can develop at the mm scale. Steep gradients in redox conditions can result in very rapid increases in Cr reduction rates with depth and sharp termination of Cr diffusion fronts. Cr(III) can accumulate at very high concentrations within shallow reduction zones. Equally important, the outer, most accessible layer of contaminated aggregates may retain elevated concentrations of potentially labile Cr(VI). This type of information is needed to understand larger scale transport through soil profiles and can only be obtained through spatially resolved studies of intra-aggregate biogeochemistry.

Acknowledgments

We thank Dominique Joyner, Keith R. Olson, Fred Gadelle, Robert Giauque, Andrew Mei, and H. Scott Mountford of LBNL, and GSECARS staff for assistance. Helpful suggestions by Mark Conrad (LBNL) on the original manuscript, and by three anonymous reviewers are gratefully acknowledged. Funding for this study was provided through the U. S. Department of Energy, Natural and Accelerated Bioremediation Research (NABIR) Program, and Basic Energy Sciences, Geosciences Program, under contract No. DE-AC03-76SF00098. Use of the Advanced Photon Source was supported by the U.S. Department of Energy, Basic Energy Sciences, Office of Science, under Contract No. W-31-109-Eng-38.

Literature Cited

(1) Adriano, D. C. *Trace Elements in the Terrestrial Environment*; Springer-Verlag: New York, 1986; pp 156−180.
(2) Riley, R. G.; Zachara, J. M.; Wobber, F. J. *Chemical Contaminants on DOE Lands and Selection of Contaminant Mixtures for Subsurface Science Research*; U.S. Department Energy: Washington, DC, 1992.
(3) Rai, D.; Eary, L. E.; Zachara, J. M. *Sci. Total Environ.* **1989**, *86*, 15−23.
(4) Zachara, J. M.; Ainsworth, C. C.; Cowan, C. E.; Resch, C. T. *Soil Sci. Soc. Am. J.* **1989**, *53*, 418−428.
(5) Eary, L. E.; Rai, D. *Environ. Sci. Technol.* **1988**, *22*, 972−977.
(6) Pettine, M.; Millero, F. J.; Passino, R. *Marine Chem.* **1994**, *46*, 335−344.
(7) Elovitz, M. S.; Fish, W. *Environ. Sci. Technol.* **1994**, *28*, 2161−2169.
(8) Wittbrodt, P. R.; Palmer, C. D. *Environ. Sci. Technol.* **1995**, *29*, 255−263.
(9) Wittbrodt, P. R.; Palmer, C. D. *Environ. Sci. Technol.* **1996**, *30*, 24−263.
(10) Bidoglio, G.; Gibson, P. N.; O'Gorman, M.; Roberts, K. J. *Geochim. Cosmochim. Acta* **1993**, *57*, 2389−2394.
(11) Anderson, L. D.; Kent, D. B.; Davis, J. A. *Environ. Sci. Technol.* **1994**, *28*, 178−185.
(12) Ilton E. S.; Veblen, D. R. *Geochim. Cosmochim. Acta* **1994**, *58*, 2777−2788.
(13) White, A. F.; Peterson, M. L. *Geochim. Cosmochim. Acta* **1996**, *60*, 3799−3814.
(14) Patterson, R. R.; Fendorf, S.; Fendorf, M. *Environ. Sci. Technol.* **1997**, *31*, 2039−2044.
(15) Peterson, M. L.; Brown, G. E.; Parks, G. A.; Stein, C. L. *Geochim. Cosmochim. Acta* **1997**, *61*, 3399−3412.
(16) Loyaux-Lawniczak, S.; Refait, P.; Ehrhardt, J. J.; Lecomte, P.; Genin, J.-M. R. *Environ. Sci. Technol.* **2000**, *34*, 438−443.
(17) Deng, B.; Stone, A. T. *Environ. Sci. Technol.* **1996**, *30*, 463−472.
(18) Deng, B.; Stone, A. T. *Environ. Sci. Technol.* **1996**, *30*, 2484−2494.
(19) Buerge, I. J.; Hug, S. J. *Environ. Sci. Technol.* **1999**, *33*, 4285−4291.
(20) Lovley, D. R.; Phillips, E. J. P.; Lonergan, D. J., *Environ. Sci. Technol.* **1991**, *25*, 1062−1067.
(21) Chapelle, F. H. *Ground Water Microbiology and Geochemistry*; John Wiley and Sons: New York, 1992.
(22) Lovely, D. R. *Annu. Rev. Microbiol.* **1993**, *47*, 263−290.
(23) Losi, M. E.; Amrhein, C.; Frankenberger, W. T., Jr. *Environ. Toxicol. Chem.* **1994**, *13*, 1727−1735.
(24) Chen, J. M.; Hao, O. J. *Crit. Rev. Environ. Sci. Technol.* **1998**, *28*, 219−251.
(25) Fendorf, S.; Wielinga, B. W.; Hansel, C. M. *Int. Geol. Rev.* **2000**, *42*, 691−701.
(26) Coats, K. H.; Smith, B. D. *Soc. Petroleum Eng. J.* **1964**, *4*, 73−84.
(27) van Genuchten, M. Th.; Wierenga, P. J. *Soil Sci. Soc. Am. J.* **1976**, *40*, 473−480.
(28) Amacher, M. C.; Selim, H. M. *Ecological Modelling* **1994**, *74*, 205-230.
(29) Jardine, P. M.; Fendorf, S. E.; Mayes, M. A.; Larsen, I. L.; Brooks, S. C.; Bailey, W. B. *Environ. Sci. Technol.* **1999**, *33*, 2939−2944.
(30) Griffioen, J. W.; Barry, D. A.; Parlange, J.-Y. *Water Resour. Res.* **1998**, *34*, 373−384.
(31) Tokunaga, T. K.; Sutton, S. R.; Bajt, S.; Nuessle, P.; Shea-McCarthy, G. *Environ. Sci. Technol.* **1998**, *32*, 1092−1098.
(32) Patrick, W. H., Jr.; Gambrell, R. P.; Faulkner, S. P. *Methods of Soil Analysis, Part 3-Chemical Methods*; Sparks, D. L., Page, A. L., Helmke, P. A., Loeppert, R. H., Soltanpour, P. N., Tabatabai, M. A., Johnston, C. T., Sumner, M. E., Eds.; Soil Sci. Soc. Am., Inc.: Madison, WI, 1996; pp 1255−1273.
(33) Bartlett, R. J.; James, B. R. *Methods of Soil Analysis, Part 3-Chemical Methods*; Sparks, D. L., Page, A. L., Helmke, P. A., Loeppert, R. H., Soltanpour, P. N., Tabatabai, M. A., Johnston, C. T., Sumner, M. E., Eds.; Soil Sci. Soc. Am., Inc.: Madison, WI, 1996; pp 683−701.
(34) Manceau, A.; Charlet, L. *J. Colloid Interface Sci.* **1992**, *148*, 425−442.
(35) Bajt, S.; Clark, S. B.; Sutton, S. R.; Rivers, M. L.; Smith, J. V. *Anal. Chem.* **1993**, *65*, 1800−1804.
(36) Kendig, M. W.; Davenport, A. J.; Isaacs, H. S. *Corrosion Sci.* **1993**, *34*, 41−49.
(37) Szulczewski, M. D.; Helmke, P. A.; Bleam, W. F. *Environ. Sci. Technol.* **1997**, *31*, 2954−2959.
(38) Bohn, H. L.; McNeal, B. L.; O'Conner, G. A. *Soil Chemistry*; Wiley-Interscience Publ.: New York, 1979; 329 p.
(39) Masscheleyn, P. H.; Pardue, J. H.; DeLaune, R. D.; Patrick, W. H., Jr. *Environ. Sci. Technol.* **1992**, *26*, 1217−1226.
(40) Sedlak, D. L.; Chan, P. G. *Geochim. Cosmochim. Acta* **1997**, *61*, 2185−2192.
(41) Pettine, M.; D'Ottone, L.; Campanella, L.; Millero, F. J.; Passino, R. *Geochim. Cosmochim. Acta* **1998**, *62*, 1509−1519.
(42) Vitale, R. J.; Mussoline, G. R.; Petura, J. C.; James, B. R. *J. Environ. Qual.* **1994**, *23*, 1249−1256.
(43) Grundl, T. J.; Macalady, D. L. J. *Contaminant Hydrology* **1989**, *5*, 97−117.
(44) Matia, L.; Rauret, G.; Rubio, R. *Fresenius J. Anal. Chem.* **1991**, *339*, 455−462.

Received for review January 10, 2001. Revised manuscript received May 21, 2001. Accepted May 21, 2001.

ES010523M